Development of high throughput microscope mode secondary ion mass spectrometry imaging

Running title: High throughput microscope mode SIMS

Felicia M Green*[1], M. Elena Castellani[2], Yifeng Jia[2], Anya Eyres[2], Natasha Smith[2], Steve Thompson[3], Paul Blenkinsopp[3], Michael Burt[2], Claire Vallance[2], Josephine Bunch[1], Zoltan Takats[1], Mark Brouard[2].

1. The Rosalind Franklin Institute, Harwell Campus, Didcot, OX11 0QX, UK
2. Department of Chemistry, University of Oxford, 12 Mansfield Road, Oxford, OX1 3TA, UK
3. Ionoptika Ltd, Unit B6 Millbrook Close, Chandler's Ford, Eastleigh, SO53 4BZ, UK

* Address reprint requests to:

Dr Felicia M Green,

Rosalind Franklin Institute, Harwell Campus, Didcot, OX11 0QX, United Kingdom,

00 447815 802501

Felicia.Green@rfi.ac.uk

Abstract

This paper describes the development and initial results from a secondary ion mass spectrometer coupled with microscope mode detection. Stigmatic ion microscope imaging enables us to decouple the primary ion (PI) beam focus from spatial resolution and is a promising route to attaining higher throughput for mass spectrometry imaging (MSI). Using a commercial C_{60}^{+} PI beam source, we can defocus the PI beam to give uniform intensity across a 2.5 mm^2 area. By coupling the beam with a position-sensitive spatial detector we can achieve mass spectral imaging of positive and negative secondary ions (SIs), which we demonstrate using samples comprising metals and dyes. Our approach involves simultaneous desorption of ions across a large field of view, enabling mass spectral images to be recorded over an area of 2.5 mm^2 in a matter of seconds. Our instrument can distinguish spatial features with a resolution of better than 20 µm, and has a mass resolution of > 500 at 500 u. There is considerable scope to improve this and through simulations we estimate the future performance of the instrument.

Introduction

With the increasing need for the microscopic characterization of biological compounds and tissues, new imaging techniques and instruments are required to ensure fast data acquisition. In mass spectrometry imaging (MSI), in particular, a given analyte can be visualized label-free depending on its chemical composition and spatial distribution. Depending on the size of the imaged area, MSI can be performed either in microprobe or microscope mode, in each case generating a 'data cube' of intensities as a function of the spatial coordinates *x* and *y* and the mass coordinate u. In microprobe mode, a tightly focussed probe beam analyses a small portion of the sample before moving to a new spot on the sample. In this case, the data cube is generated by scanning across the surface and recording mass at each point in a grid of (*x*,*y*) locations. In microscope mode, the whole analyte surface is illuminated and electrostatically projected onto a position-sensitive detector paired with a fast camera. This latter approach exploits a position-sensitive detector, stigmatic ion optics to preserve the spatial distribution of the ions as they travel to the detector, a defocussed probe to generate ions from a large surface area, and an ultrafast and a position-sensitive detection system capable of recording time-resolved (assuming a time-of-flight mass filter) and position-resolved ion signals. Each pixel of the camera corresponds to an individual mass spectrum. Microscope-mode MSI records the whole mass spectral image in a single measurement, in contrast to recording the image pixel by pixel as in microprobe mode. This enablesrapid imaging of the many chemical constituents present at a surface, as well as decoupling acquisition time from spatial resolution. Of course, this assumes a similar signal to noise ratio to achieve similar images with a single scan. Two important contributions are the primary ion current and detector sensitivity. A focussed PI beam generally requires cutting the PI current, so a defocussed beam is advantageous, however some SIMS instruments[1] use an unpulsed PI beam and pulse the detector and hence use much higher PI currents (nAs rather than pA). This is not easy in microscope mode due to the need to maintain spatial information. The other consideration is the sensitivity of detection, each scan in a microprobe experiment can use as many pores on the MCP and the whole scintillator to detect without limiting spatial resolution. However, the CMOS cameras used for detection can detect each individual ion event making microprobe-mode imaging a promising route to attaining MS images in a single scan or seconds rather than per pixel or over hours.

Two main ionization techniques have been used in microscope mode MSI: matrix-assisted laser desorption-ionization (MALDI); and secondary ion mass spectrometry (SIMS). Some of the initial development of SIMS in the 1960s was carried out in microscope mode [2] (or see the recent translation [3]). Later work employing SIMS exploited high-speed ion blanking before the detector [4] [5] or fast frame-transfer charge coupled device (CCD) cameras to rapidly acquire spatially-resolved MS images [6, 7]; these approaches built on earlier work by Schueler and co-workers, in which a SIMS instrument was used to record microscope ion images for a set mass window [8, 9]. These studies showed the feasibility of microscope mode MSI and the possibilities for high spatial resolution (<10 μm) and fast acquisition times. Further developments included the use of delay line detectors [10] [11] [12] to detect both the spectral and spatial information in microscope MSI simultaneously. However, the acquisition speed, mass range, and resolution

were limited by the acquisition and reconstruction efficacy of the delay-line detector. The development of complementary metal-oxide semiconductor (CMOS) image sensors with 'intelligent pixels' overcame this limitation by offering a route to a new generation of ultrafast time and position sensitive ion detectors. In such a detector, a pair of microchannel plates coupled to a phosphor screen converts the incoming ions into optical signals, which can be recorded and read out to a PC by a suitable CMOS imaging sensor.

Early work demonstrating microscope mass spectrometry using pixelated CMOS detectors mostly employed a MALDI ion source, maybe due to the ease of defocusing the light over the examined area. The detectors were generally specifically designed for the task. These included the pixel imaging mass spectrometry (PImMS) sensor, which can record multiple time stamps within each pixel in a two-dimensional array following a suitable trigger signal [13-15], and implementations of the Timepix [16] readout system which enables the time of flight of a particle to be detected relative to a trigger signal [17]. Early studies combining MALDI and a triple focusing time of flight (TRIFT) detector (that uses blanking to select specific ion ranges to maintain the mass resolution) with Timepix could achieve 6 µm spatial resolution over an area of a few hundred microns and up to masses of 78 kDa [18, 19]. Further work increased the upper mass limit in microscope-mode MALDI imaging first to 100 kDa [20], and later to 400 kDa [21], before more recently achieving 800 kDa [22] with the use of a time of flight mass analyser. Only a few examples of microscope mode imaging mass spectrometry with CMOS detectors have used a SIMS approach, in which a high energy (~20keV) charged ion beam desorbs and ionises molecules from a surface [23, 24,17]. Kiss *et al.*, using linear time-of-flight (ToF) mass separation and a Timepix detector, achieved a spatial resolution of 5 - 7 µm over an area of approximately 200 x 200 μm^2. They noted that increasing the acceleration voltage used to extract the secondary ions (SIs) increased both the intensity and signal-to-noise ratio of the detected ion signal. However, the mass analyser used in this work required peak selection, and the early-generation Timepix camera employed was only able to run at 30 Hz, making image acquisition of multiple ion species rather time consuming. Halford *et al.* used laser desorption ionisation (LDI) and a ToF mass analyser. The detector was a dual MCP/phosphor screen ion detector coupled through an optical fibre bundle and a lens to with a PImMS camera situated outside of the vacuum chamber - to enable simultaneous detection of mass spectrum within each pixel (with a possible maximum of four ion arrival time recordings per pixel per experimental cycle) and this was initially able to achieve unit mass resolution over a broad (300-800 u) range of masses [25]. Development of the ion optics to include at first a double pulsed extraction [26], and then a time-variable extraction field [27] led to an improvement in the mass resolution to 2700 over an increasingly broad range of masses while maintaining 22 µm spatial resolution. The addition of a reflectron and a faster scintillator was able to enhance the mass resolution further to over 8100 with a spatial resolution of 18 µm [28] and it has been shown the number of reflective lenses could potentially be increased indefinitely to improve the mass resolution further [29]. Guo [27] was also able to show that much higher mass resolution (~30,200) and sub- 10 µm spatial resolution would be achievable if several practical experimental limits were overcome.

In the following, we describe the construction of a stigmatic imaging SIMS instrument that combines these various advantages. The instrument employs a broadly defocussed 40 keV

C_{60}^{+} primary ion (PI) beam, extraction lens optics that are capable of accelerating the secondary ions up to 20 keV, a time-variable pulsed extraction potential, and a pixelated detector for the detection of both positive and negative ions. The new instrument will allow rapid molecular mapping of surfaces with unprecedented speed, while at the same time offering spatial resolution, mass range, and mass resolution comparable to microprobe instrumentation.

Experimental

We describe the development and construction of a stigmatic imaging SIMS instrument, which is capable of rapid molecular mapping of large areas (> 2 mm^2) with > 1000 mass resolution across a broad (1000 u) mass range. Key design criteria included a primary ion beam that will desorb intact molecules, the ability to compensate for the energy distribution of the secondary ions, and the ability to mount different cameras relatively easily. The instrument is comprised of a 40 keV C_{60}^{+} PI gun, a sample stage, extraction optics, a time-of-flight (ToF) tube, and a detector assembly, all housed within a high vacuum system; then the camera mounted in the atmosphere above the phosphor screen. Details of the instrument design are shown in Figure 1 with the overall instrument setup as the schematic in Figure 1 (a). Elements of the instrument design will be discussed in detail as considered in the results section for the 3 different regions. Details of the 3 different areas of Figure 1 (a) are shown in more detail in Figure 1 for (b) the primary ion beam column; (c) the SI extraction optics; (d) the detection and identification capability.

All simulated data was obtained using using the software packages SIMION 7.0 or SIMION 8.0, modelling software that allows ion trajectories within electromagnetic fields to be carefully calculated[30]. Two models were used, separately and integrated together, the first incorporating the end of the C_{60}^{+} ion column to the sample stage in order to map the PI beam. The second incorporating the ion optics from the sample stage to the front plate MCP of the detector, in order to investigate the SI beam and calculate mass and spatial resolutions. Calculations of mass and spatial resolution were based on a distribution of SI velocities appropriate for C_{60}^{+} sputtering and are detailed later

Different metal samples were purchased from Agar Scientific Ltd, surface cleaned by ultrasonic for 1 minute in isopropanol, N_2 dried and then mounted onto a conductive sample stage before entering the sample chamber vacuum. Rhodamine B samples were prepared by spraying a solvent mixture onto an indium tin oxide (ITO) slide. Grid patterns were formed using a metal mesh to mask areas of the slide. These slides were also mounted onto a conductive sample stage before entering the sample chamber vacuum. Sample height relative to the extraction optics and PI beam was kept constant, with a 1.5 mm separation between the sample stage and extraction plate, Figure 1 (b).

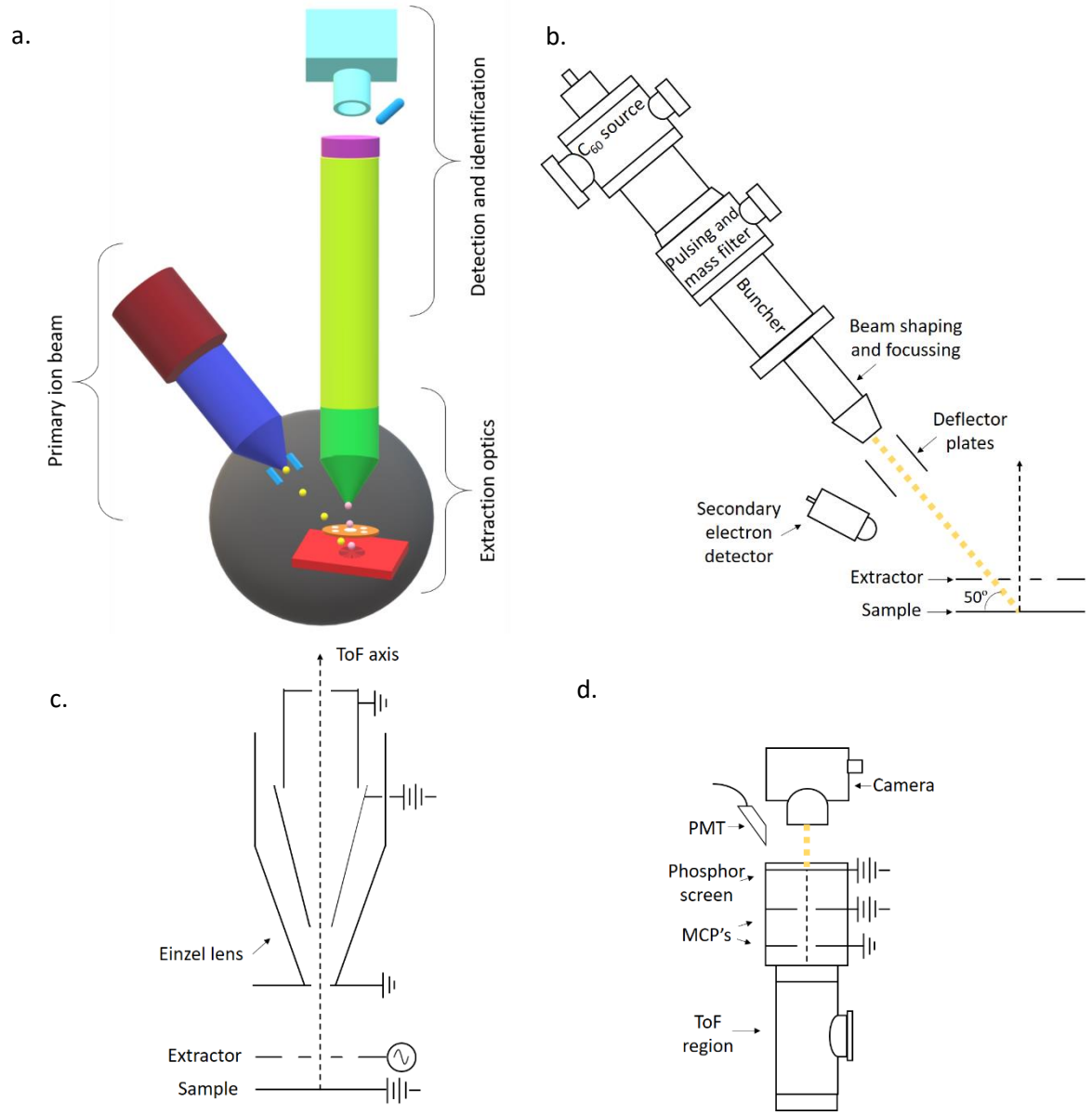

Figure 1 – A simplified schematic showing the basic components making up the microprobe SIMS instrument. An overview of the complete instrument and the connection between the different regions are illustrated in (a). Details of each section, shown as schematic cross sections in the vertical plane, for: (b) the primary ion beam optics; (c) the extraction optics; (d) the detection and camera setup.

Results and Discussion

Primary ion beam

A buckminsterfullerene (C_{60})-based primary ion beam system has been used for the SIMS, this ion beam system has been described, and its performance characterized in detail elsewhere[31]. The usage of cluster PI beams in SIMS can effectively increase the intensities of intact

molecular ions detected [32]. This has made the analysis of complex molecules with SIMS more attractive and provided the scope for SIMS to be used to directly study biological samples [33-35].

A schematic of the primary ion beam is shown in Figure 1(b), with a simplified overview of the features used to ensure a clean, short pulse of ions hit the sample. Note the column sits at a 50 degree angle to the sample surface (shown in Fig. 1(b)) at an approximate distance of 30 mm. In brief, a solid source of C_{60} is heated and evaporates, these molecules are ionised using electrons produced from a filament to mostly become C_{60}^{+}, but some proportion forms C_{60}^{++} and C_{60}^{+++}as well as isoptopic variants. A Wien filter separates these and a 1 degree bend removes neutrals. The ions are accelerated to up to 40 keV and pulsed to achieve ToF-SIMS. Running at a repetition rate of 20 Hz, limited by the repetition rate of the CMOS camera, yields a primary ion beam current of around 1 pA at the sample surface. Ion optics are used to shape and focus the PI beam through the column to achieve a regular sub-micron spot at the sample. To ensure a sharp pulse, there is a chamber with front and rear electrodes that can compress the initial beam pulse width of ~ 100 ns and achieve an ~ 1 ns pulse of C_{60}^{+} ions at the surface. Using a polyatomic C_{60}^{+} PI beam can reduce sample surface damage relative to other commonly used primary ion beams while maintaining a high sputtering rate [31, 36]. As a result, a greater proportion of the ions produced from the surface are characteristic of the sample composition, and the sample can be bombarded for a longer period of time without a loss in the formation of characteristic ions.

Microprobe SIMS analysis uses an energetic, highly focussed PI beam (< 500 nm spot size) for high-resolution sputtering to produce SIs for analysis. The beam is scanned across the surface, with SI mass spectra recorded at each position, until the whole area of interest has been covered. In contrast, microscope mode SIMS enables imaging of all SIs from the area of interest simultaneously, generating mass and spatial information at the same time. An important first step towards microscope mode SIMS is therefore the production of a uniform defocussed PI beam to irradiate the surface area to be analysed.

The geometry of the instrument is designed such that the PI beam hits at the point of intersection between the sample and the ToF axis. To reach the surface the PI beam must pass through the SI extraction plate, Figure 1 (b). To enable this a 2 mm diameter hole has been bored into the extraction plate to allow the PI beam to pass through to the surface. The PI beam hits at the region of the surface directly in line with the ToF path of the SI's - this goes perpendicular to the surface, through the extraction optics and up to the detection region. To extract SIs from the surface into the ToF analyser, high voltages are applied to the sample stage and extraction plate. The polarity of the field is switched between negative or positive depending on whether extraction of negative or positive SI's is required. The trajectory of the C_{60}^{+} beam is affected by the potentials applied to the extraction ion optics, and is affected differently depending on whether these are set for the extraction of positive or negative secondary ions. A set of deflector electrodes at the end of the PI column, Figure 1 (b), enable these effects to be corrected, allowing the PI beam to be steered to the desired position on the sample surface regardless of the extraction field settings. By careful modelling of the ion trajectories using the SIMION 8.0 software package [30], we have been able to optimize the use

of these deflector plates to guide the PI beam through the extractor while remaining central to the detection optics. These simulations show the necessity of including deflector plates in order to achieve positive and negative SI detection.

The position of the primary ion beam on the surface can be measured experimentally. Using a sample surface of copper tape, marks can be made with the C_{60}^{+} PI beam under different voltage conditions, then subsequently measured with the same geometry, but no applied voltage. Imaging of these marks is carried out using a secondary electron detector (SED), Figure 1(b), to detect the electrons formed when scanning the C_{60}^{+} PI beam across the area of interest (effectively microprobe mode imaging). Ablation of a metal surface by the PI removes surface contaminants that ionise easily and so appear brighter in the secondary electron image. By using the SED, we can visualise the marks relative to the PI beam position under no electric field (hence aligned to the SI axis). Measurement of these marks can explore the positional shift of the PI beam under different voltage conditions and compared to simulated data from SIMION.

Figure 2 (a) displays the use of the PI deflector plates to move the PI beam position on the sample surface relative to the SI detector optics. The calculated experimental shifts of the marks and hence PI beam using the deflector plates, is shown alongside those simulated. The experimental effect of varying the potentials applied to the deflector plates somewhat matches that seen in the simulation. However, there is a slight systematic shift in the experimental data such that the deflectors seem to have slightly less effect than in the simulation. One reason could just be that the voltage supply is miscalibrated, such that slightly less voltage is being applied than expected. Another cause could be a slight difference in geometry caused by real world variance in the position of the electrodes. Using SIMION, we can test a few scenarios to see what the impact would be. Absolute shifts in distance and voltage would change the deflection of the beam by a systematic amount across the voltage range, as would shifts in the ion beam position or angle. However, a skew of the stage, such that it is tilted relative to the rest of the ion optics, would also give this effect. Simulations of the deflection arising when the stage is at a tilt of 7.5 degrees are marked in Figure2(a) as blue crosses, and bring the simulation results directly in line with those from the experiment. Shifts in the PI beam position can be measured when the sample stage and extraction plate voltages are varied. Matching these shifts, and through SIMION, we can calculate the potentials required on the deflectors for given extraction conditions, ensuring the PI beam remains central to the extraction optics.

Deflection optics embedded in the PI column usually used to raster the beam (move it back and forth) over the sample surface are not required experimentally in microscope mode. Therefore, we can use them to give us further capability to deflect the beam. Figure 2 (b)-(d) shows their experimental effect on the PI beam position, both measured (b) and shown as SED images of the burn marks in (c) and (d) (note *y* has been rotated). Figure 2 (b) shows the clear linear movement of the beam on the surface with a change in the raster controls. By measuring the shift of the burn marks shown in Figures 2 (c) and (d), we can predict the translational shift of the ion beam for a specified value. This gives us experimental flexibility and control over the placement of the PI beam relative to the detector. This is important to

allow us to make minor adjustments for any slight error or skew in the beam or extraction optics, that would otherwise prevent us from seeing the full beam width or detecting the available SIs.

It is clear from both simulations and experiments that we need to be careful to optimise the position of the PI beam relative to the ToF axis, and therefore the centre of the detector, and not just optimise the PI beam to pass through the hole in the extractor plate on the way to the sample surface. If the beam is not within the frame of view of the detector, then the sputtered SIs from this region will not reach the detector, and therefore will not be detected. This is critical as we consider a defocussed PI beam which can potentially be clipped by the edges of the holes in the extraction plate, as can the SI's on their trajectory to the detector if the PI beam is not appropriately centred on the sample.

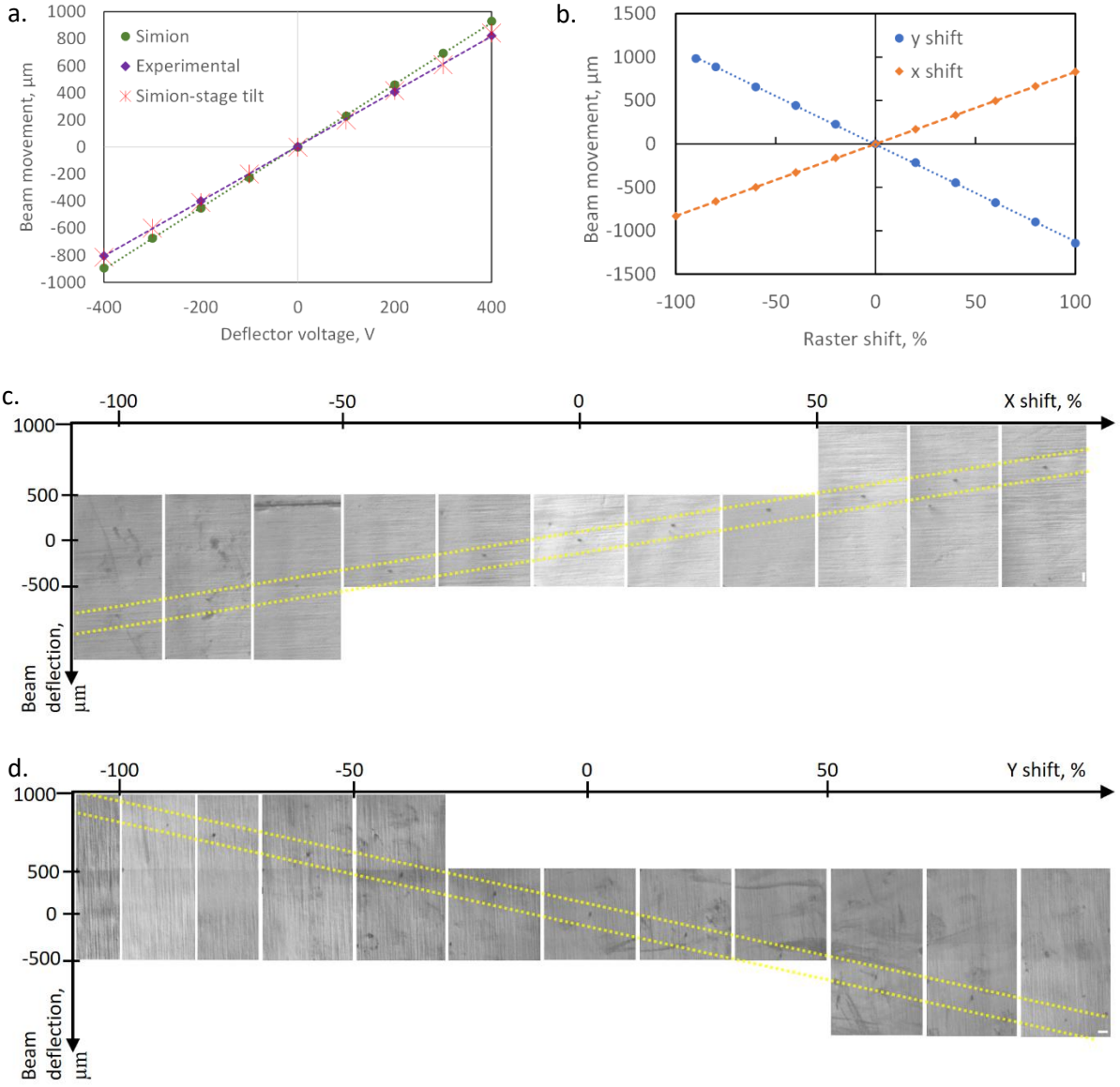

Figure 2 (a) Experimental (purple, red crosses with a stage tilt of 7.5 degree) and simulated (green) PI beam position on the sample. (b) Experimental PI beam shifts with % of rastering deflector in x and y. The dashed lines show linear fits to the data. Experimental data is an average of 3 replicates with a standard deviation of ~10 %. (c) and (d) show the raster x (rotated 90°) and y shifted PI spots on a copper surface, images taken with a secondary electron detector (SED). Circles and dashes to guide the eye. The white scalebar is 100 µm.

Images of the marks made by the PI beam can give us an experimental measure of the area probed by the PI beam. To defocus the PI beam before it hits the surface we use the final focussing ion optics at the end of the PI column, as shown in Figure 1(b). Figure 3 shows that the PI beam is gradually defocused as the potential applied to the final lens optic is reduced. SED images of the marks are displayed in Figure 3 (a-g) the lens set to potentials between 0 kV and 17 kV. The associated beam diameters measured from these marks are indicated in Figure 3 (h). As the beam diameter increases, we see interference from the extractor plate (as seen in Figures 3 (a-e). This appears as a circular "edge" with a consistent pattern cutting off the top of the PI beam, due to the extractor plate blocking the PI beam from reaching the surface to mark it. We could shift the PI beam position relative to the extractor plate using the deflectors, however, then the PI beam would become blocked at the bottom – this can just be seen in the image in Figure 3 (a). This gives limitations yet we show that we can obtain a maximum spot size of 2.5 mm^2, which is a 100 times improvement on earlier stigmatic SIMS experiments, which used a beam of a width of 0.024 mm^2 [23]. These previous experiments were unable to sample a wider area due to the use of a TRIFT mass spectrometer, where the maximum acceptance area of the SIMS extraction optics is limited to enable transmission through the triple focusing optics. A more recent study[37] was able to sample larger areas but by combining the stigmatic mode with scanning of the surface (microprobe mode). Simulations at lower PI energies suggest that the spot size could potentially be increased to ~20 mm^2, and without the extractor plate in the way, the C_{60}^+ PI beam would be able to cover a surface area greater than 3 cm^2. Of course, larger areas would not necessarily be detectable, either due to limitations in the extraction of ions from those edges, the size of the detector, or the reduction in sensitivity. To enable larger areas to be visible at the detector, you could use magnifying optics to reduce the spatial range of the projected ions entering the extraction region or hitting the detector. However, larger areas may also contribute a broader range of time of flight differences in the ions and a poorer mass resolution.

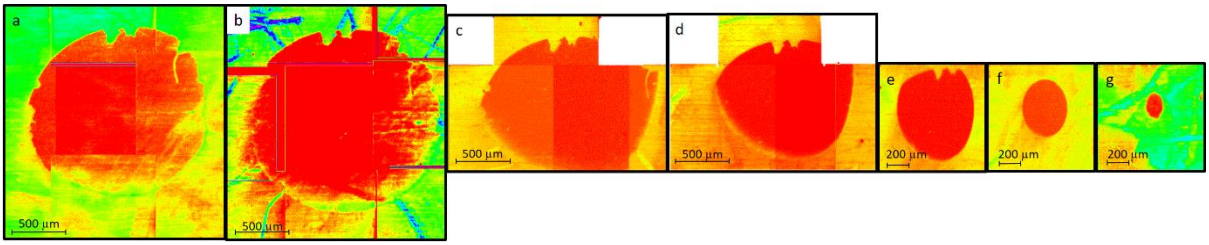

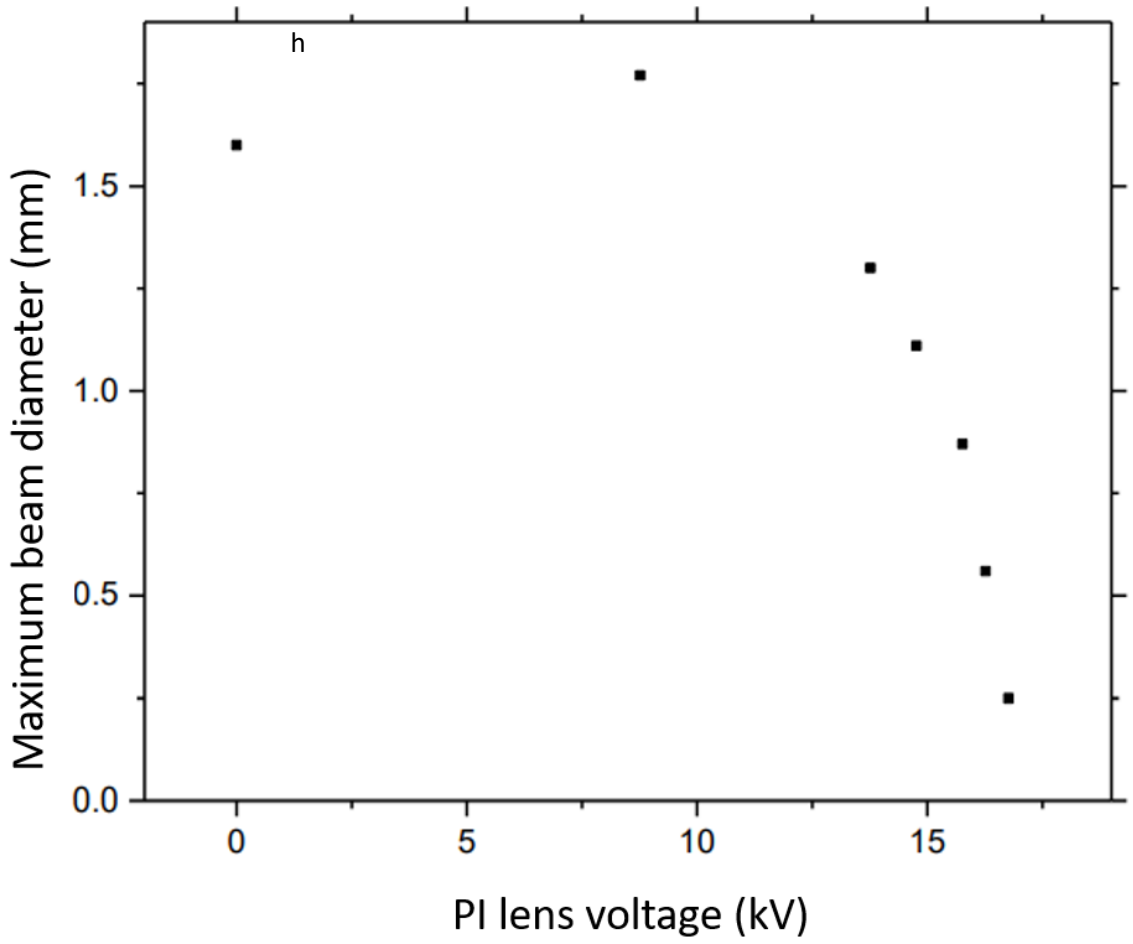

Figure 3. "Burn" marks are produced when a C_{60}^{+} PI beam impacts a copper surface, the figures (a) to (g) show SED images of the burn marks made with decreasing focusing lens voltages. Some images have been collated together from several SED scans at differing positions. The changing spot size is clear and measurements of the spot diameter taken from these images are shown in the graph in Figure(h). A false colour range has been used to enhance the image.

Of course, imaging across a large area requires the defocussed PI beam to desorb ions uniformly across the beam spot, such that peak intensities in can be compared from different regions of the sample. The marks shown in Figure 3 only show the effect of the PI beam after 5 minutes, but the approach is too crude to give a clear indication as to the uniformity of the beam. Assessing this requires measuring the ion flux, that is PI beam current per unit area, at different positions within the defocussed PI beam spot. To do this we employed a modified Faraday cup, illustrated schematically in Figure 4(a). The device consists of a pinhole in a thin metal sheet, which is mounted above a metal sample connected to an ammeter. By scanning the pinhole over the area of the incoming beam, the spatial dependence of the beam current can be measured. Figures 4 (b) and 5 (c) show the ion flux for a mid-focussed (0.18 mm wide) and a defocussed (1.8 mm wide) C_{60}^{+} PI beam, respectively. The range of currents measurable in Figure 4 (b) – up to ~2000 pA confirms that the plateau at ~20 pA seen in Figure 4 (c) as green is not due to a saturation in the signal. These data show that the beam can be defocused in a uniform manner, creating a broad ion beam of even flux.

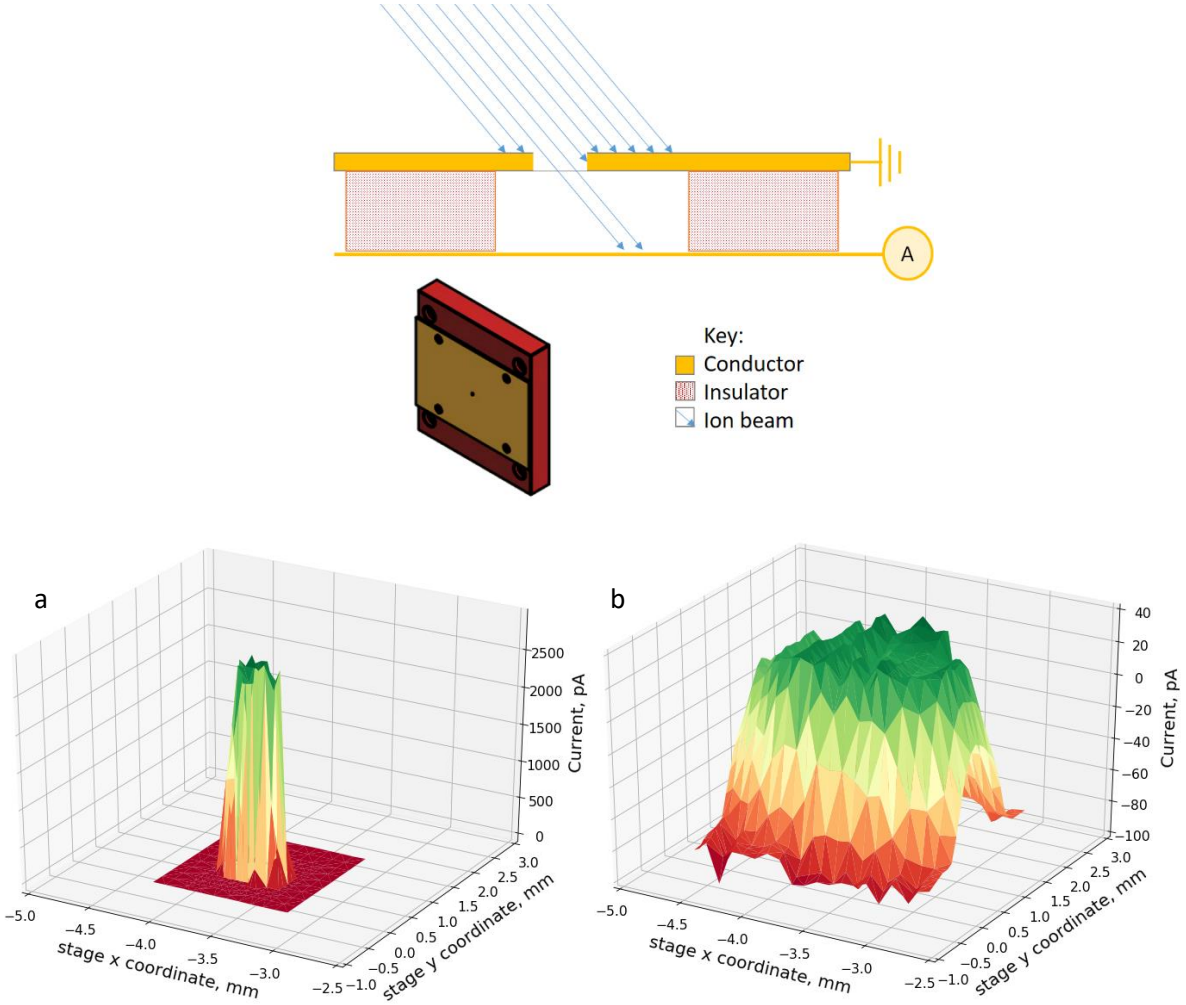

Figure 4. (a) Schematic of a device based on a faraday cup for measuring beam flux at a given position. Current beam profile for a C_{60}^{+} PI beam when (b) partially focussed (0.18 mm wide) and (c) fully defocussed (1.8 mm wide).

Extraction optics

The SIMS sputtering process can be quite energetic, leading to the emission of SIs with a broad velocity distribution. This range of initial velocities, when coupled with ToF mass analysis, can lead to a spread of arrival times at the detector for an ion of a given mass, resulting in a broad peak in the mass spectrum and an overlap of signals for ions with similar masses. The mass resolution achieved in a given measurement is calculated for a given mass as the mass at the peak centre (m) divided by the full width half maximum (FWHM) of the peak (Δm). Several approaches can be used to minimise the effect of the secondary ion energy distribution on the mass resolution, including the use of delayed extraction [38], the inclusion of a reflectron in the instrument [39], and peak fitting of the measured spectra [40]. In microprobe mode MS, a delayed extraction works by using an electric field that can be pulsed on at a precisely determined time after the PI beam sputtering to refocus the time spread of the SIs [38]. However, in microscope-mode ToF-SIMS, the positions at which the secondary ions are created needs to be preserved throughout the extraction, yet a delayed extraction allows the

SI's to disperse, blurring the detection of their original position. The use of a variable electric field to extract and accelerate the SIs, rather than a delayed extraction, can reduce the blurring effect and compensate for the effect of SI energies on the mass resolution [27, 41]. Gao *et al.* continued the work by Aoki *et al.* to show that a pulsed extraction field creates a temporal focal point that can be optimised to correct for the spread of SI velocities. This correction can be achieved both for a single specific mass or across a range of masses. In the former case, a mass resolution of ~3,000 was achieved for a mass of 410 u [26]. More recently, a time-dependent post extraction differential acceleration (PEDA) field was shown to enable the mass resolution to be optimised over a range of masses, achieving a mass resolution of better than 2500 over the mass range from 300-600 u [27].

To extract SIs from the surface into the ToF analyser, our new instrument allows high voltages to be applied to the sample stage and extraction plate before an Einzel lens focuses the SI onto the detector, as shown schematically in Figure 1(c). The polarity of the field is chosen as appropriate to obtain negative or positive ion mass spectra. The extraction optics and electronics enable a time-dependent potential to be applied to the extraction plate, giving us the potential ability to achieve excellent mass resolution over a broad mass range. To allow maximum flexibility, the electronics have been designed to allow acquisition at a repetition rate of 10 kHz for both positive and negative SIs.

SIMION models of the secondary ion trajectories through the extraction optics shown in Figure 1 (c) can be used, both to optimize the voltages and time delays used for pulsed extraction of the SIs, and to explore the instrumental possibilities and limitations. The energy/velocity distribution of the SIs produced in SIMS is one of the key factors that determine the spatial and temporal distribution of the ions at the detector. To simulate this we used a Boltzmann distribution of initial kinetic energies (peaking at 1eV), based on the extraction energy of sputtered gold particles [42] and a $cos^{12}(\theta)$ angular distribution [43] based on experimental data for nickel sputtered by C_{60}^{+} [44]. Optimising the mass and spatial resolution of the SIMS instrument via the SIMION simulations was achieved using a mixture of two methods, a gradient search and a genetic algorithm (GA).

In Figure 5, we focus on two different SI extraction types applied to the extraction plate (whose position relative to the surface is shown in Figure 1(c)). Firstly a fixed, static field (shown in Figure 5 (a) as orange hollow circles on a dashed line) and an extraction field that is increased by a single step voltage at an optimized time (referred to here as a single field (SF)). The GA was employed in the simulations of the SF to identify the instrumental parameters yielding the best mass resolutions for each particular ion in the mass range from 200 u to 1400u, shown as the red dashed line with hollow triangles in Figure 5 (a). The effect of the phosphor screen rise time on the mass resolution was also examined by including the phosphor screen rise time for the P47 screen used currently in our instrument into the simulations, namely 6.7 ns. Convoluting this rise time with the optimized SIMION results is seen to have a significant effect on the achievable time resolution, as shown by the solid lines in Figure 5 (a) and (b). The phosphor screen and other components of the detection system are certainly worthy of further optimisation. Comparing now the fixed-field and stepped-field extraction regimes, we see that the time resolution can be improved by almost a factor of ten

by implementing stepped-field extraction. Though note that this required reoptimisation at each mass.

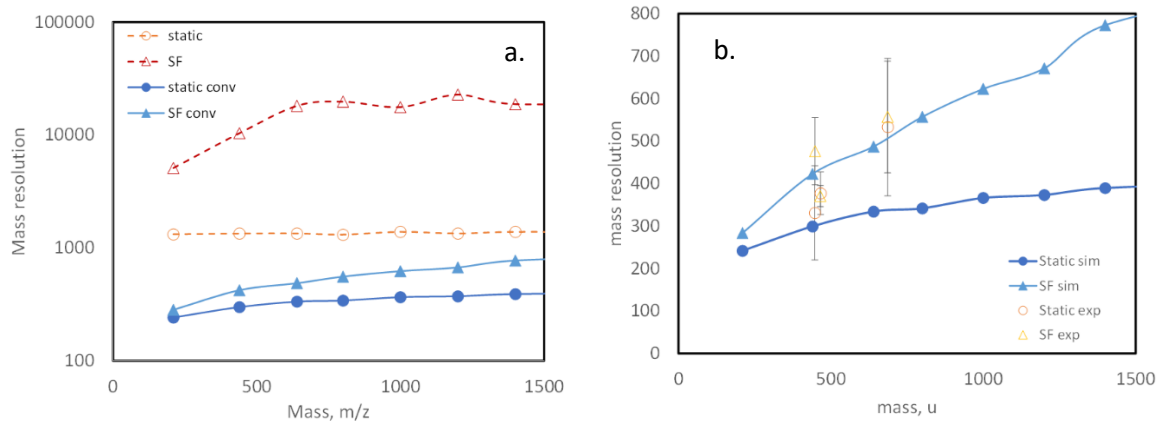

Figure 5. Simulated results for the optimized mass resolution under both static and single field (SF) pulsed extraction. (a) The simulated resolution with (solid lines) and without (dashed lines) convolution with a 6.2 ns rise time as currently expected experimentally. Note the log scale on the y-axis. (b) The simulated results (solid lines) in comparison to experimental data (outline markers show an average value of three spectra with error bars showing the standard deviation) from negative Ta spectra for the peaks of $Ta_2O_6^-$ and $Ta_3O_9^-$.

Detection and identification

The detector assembly used here, shown schematically in Figure 1 (d), is set after a tof region of 0.9 m and is comprised of a dual microchannel plate (MCP) stack coupled to a phosphor screen. The dual MCPs amplify the secondary ion signal via an electron cascade, which is then converted to an optical signal when the electron bursts generated by each ion impinge on the phosphor screen. The detector assembly (Photonis 39042PS-P47) consists of two 40 mm imaging quality Chevron™ MCPs and a fiberoptic phosphor screen with P47 phosphor mounted to a 6" vacuum flange. The MCPs are run with the front of the first plate at the ground, the back of the first plate electrically connected to the front of the second plate, and the back of the second plate set at 1.5-1.8 kV. The phosphor screen is set at 5-5.8 kV and is set up such that the light is emitted into atmospheric pressure. The photon signal from the screen can be detected and captured for subsequent analysis using either a CCD or CMOS camera (see below for details), or a photo-multiplier tube (PMT).

The main camera used in the present work is based on a PImMS1 sensor, a time-stamping CMOS device that enables position and time sensitive detection of visible light [13, 15, 45]. The PImMS1 sensor comprises an array of 72×72 pixels, each 70×70 μm in size, and can record up to four particle arrival times per pixel per scan with a timing precision of 12.5 ns. The sensor has an advantage over CCD cameras in being able to record multiple masses on each experimental cycle, and since individual pixels are triggered on detection of an optical signal, there is also no need to pre-define the times at which images must be acquired, At the end of each acquisition cycle, the data is read out and transformed into a set of (x, y, t) data points,

one for each detected ion [46]. Experiments were also carried out using, an Allied vision Manta (MG 031B ASG) CCD camera with higher spatial resolution (656 × 492 pixels) than the PImMS camera, and a RCA 1P28 fast (< 2 ns) PMT, for comparison with the PImMS data and for further characterisation of the spatial and mass resolution of the instrument. Alternative time-stamping CMOS sensors are now available, including the larger (324 × 324 pixel) PImMS2 sensor and the Timepix family of sensors [16, 47], and will be evaluated in future work.

The PImMS data sets recorded from the new SIMS instrument have been post-processed for optimum spatial and time resolution using a centroiding technique described in full elsewhere [25]. Briefly, each ion hitting the MCP's leads to a burst of electrons hitting the phosphor screen and a cluster of photons being realeased. These photons are detected by the PImMS sensors over a number of adjacent pixels and record a similar time stamp. Therefore these clusters of pixels can be assigned to a single ion event. By being able to isolate a single ion event the cluster of pixels can be centroided to improve the spatial and time resolution, larger cluster sizes will help this [25, 48]. Ideally we want to increase the event rate while minimising overlapping in order to maximize the number of events that you can isolate and measure. The response of the detector depends on the voltage applied across the MCPs, which determines the number of electrons generated per incident ion, and the voltage applied between the back MCP and the phosphor screen, which determines the number of photons emitted from the screen per incident electron. Generally, higher MCP and screen voltages increased the size of the clusters for an individual ion event, although the MCP voltage appeared to have a greater effect. However, there is an upper limit to the voltages that can be applied (2 kV) before signal saturation and/or damage to the detector occurs.

The C_{60}^{+} PI beam pulse length affects the achievable mass resolution – a 100 ns PI beam pulse without any secondary ion focussing will at best only produce a mass peak with a width of 100 ns. However, through electrostatic optics the PI beam pulse is bunched, that is as the PI beam pulse passes through the bunching chamber (Figure 1(b)), a pulse is applied to the rear electrode which compresses the pulse into a shorter time. This reduces the 100 ns pulse width to sub 5 ns [31]. Bunching the PI beam will slightly degrade the energy spread of the primary ion beam, but we see no degradation in the mass spectra so this is assumed negligible or at least small enough not to be strongly outweighed by the advantages. In the following, we will present some of the first mass spectra recorded with the new instrument. We chose to use metallic samples for our initial instrument characterisation. SIMS has long been [49], and is still, widely [50] used in semiconductor and impurity analysis. While SIMS is now more broadly used across a wide range of fields and materials, detection of metal ions is still relevant, with current studies showing exciting applications in the detection of metal tagged antibodies [51], for example. Metallic samples are also ideal for initial calibration of the ToF system due to the highly characteristic and broadly spaced mass peaks. The instrument obtained excellent positive and negative SI mass spectra for a range of metals, Figures 6 (a) and (b) show example spectra for indium recorded with the PImMS1 and photomultiplier (PMT) detectors, respectively. The spectra are broadly similar, with the same peaks in each. Yet the PMT spectra shows a larger Indium peak and smaller low mass (< 100 u) contaminant peaks, this could be due to some slight saturation on the lower mass peaks, or less sensitivity of the detector at higher masses - which leads to events being recorded by the PMT that are not

recorded by the PImMS1 camera. The mass resolution of the Indium peak is 420 for the PMT and 127 for the PImMS1 camera. Figures 6 (c) and (d) show negative and positive mass spectra recorded for aluminium with the PImMS1 detector. A number of peaks are visible in all the mass spectra including the metallic ions. Peaks identified as metallic ions arising directly from the metals themselves are labelled as well as contaminant peaks with high intensities. The negative mass spectra also include the electron and hydrogen peaks (hard to distinguish on the far left hand side of the spectra), as well as oxygen and hydrocarbons arising from contaminants at the surface. The positive mass spectra also include peaks for sodium (at 23 u), potassium (at 39 u), some silicates (at 73 u) and small organic fragments - all arising from contamination of the sample surface. Negative and positive ion metal spectra for copper, indium, tantulum and gold (not displayed here) similarly display elemental peaks as well as dimers, trimers, some oxides and some contaminants.

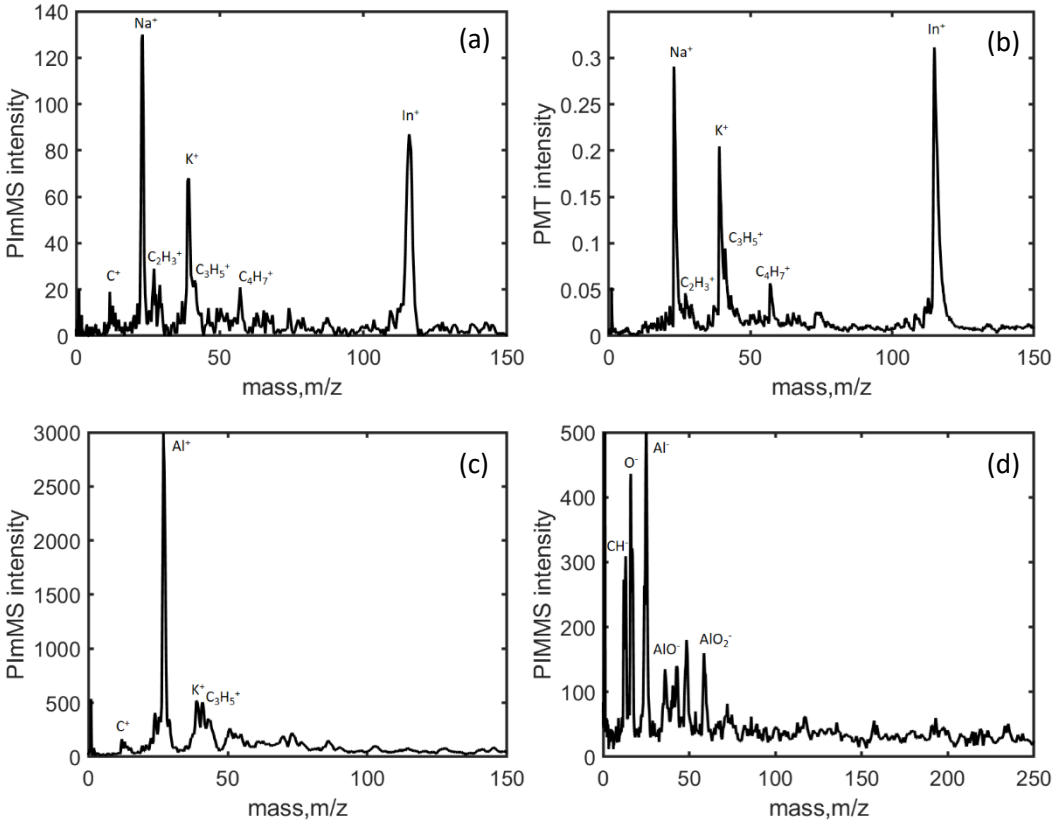

Figure 6 – SIMS mass spectra of indium acquired with (a) the Pixel Imaging Mass Spectrometry 1 (PImMS 1) camera and (b) with a photomultiplier tube (PMT). PImMS 1 SIMS mass spectra of aluminium for (c) positive and (d) negative ions.

The detector setup we are using for this paper has some limitations. The scintillator used here is a P47 layer, which has an emission peak with a 6.7 ± 0.2ns rise time and a decay rate of 168 ± 2.3ns. This will be a limiting factor if looking at the full-width half-maximum (FWHM) of an individual mass peak in order to calculate the mass resolving power of the instrument. To minimize the effect of the phosphor time response, we instead use the leading edge of the peak (20-80%) as a measure of the peak width in order to calculate the mass resolution. For initial experimental tests, we used a fast photomultiplier coupled to an oscilloscope to record mass spectra directly from the phosphor screen with greater time resolution than the 12.5ns

timing precision of the PImMS1 camera. Figure 5 (b) shows the mass resolution calculated for a range of tantalum peaks from a positive ion mass spectrum recorded using our stigmatic SIMS with the PMT detector. This shows performance using the two different SI extraction modes described above: a fixed-field extraction and a stepped extraction. Note that the trigger time for the stepped pulse was adjusted to optimize the mass resolution The comparison of the experimental and simulated data for the single pulsed field (SF) appears to be quite good, increasing with increased mass as expected. However, the mass resolution of the static data seems consistently worse than the simulated mass resolution.

To determine the spatial resolution achievable with the present extraction voltages on a larger pixel array, we record images with a CCD camera with a 656 × 492 pixel array. Figures 7(a) and (b) show SI images recorded from a surface on which Rhodamine B dye had been deposited in a grid pattern using a mesh stencil. Geometrically different meshes were used for the two images. Measurements of the 20-80 % signal intensity averaged across several of the signal edges within the grid pattern in Figure 7 (b) yield a spatial resolution of 23.8 ± 8.2 µm. SIMION simulations of the ion trajectories through the instrument with these extraction voltages predict a spatial resolution of 25 µm. These initial tests give an excellent preliminary spatial resolution with good comparability to SIMION simulations. Further evaluation and modification of the extraction optics could improve this further. In addition to a measurement of the spatial resolution of the instrument, Figure 7 also gives an indication of how much of the area sputtered by the PI beam can be imaged at the detector with the current magnification (a factor of 7-8). The image in Figure 7 (b) shows a grid of pitch 140 µm. We observe ~11 x 11 grid squares in the image, which corresponds to a detected area of ~1.86 mm^2. This is ~75% of the defocussed PI beam incident on the surface, as seen in Figure 3. Some ion losses are expected during the extraction and flight, due to apertures within the extraction optics, but with adjustment of the positioning of the extraction optics and of the SI lens focussing optic - in order to change the magnification factor - these may be minimised and it may be possible to detect a larger area.

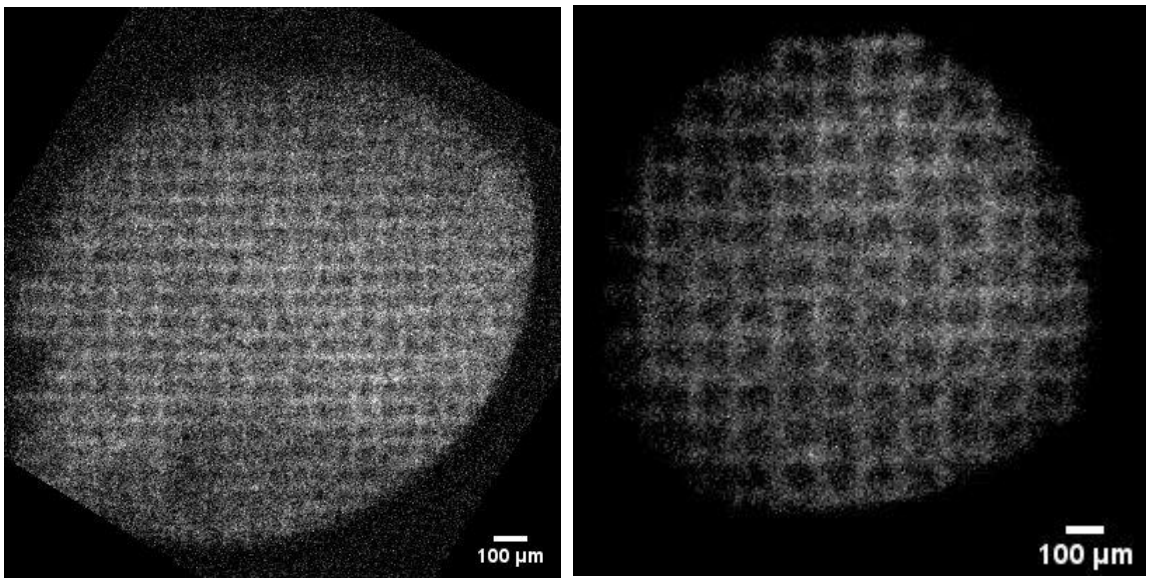

Figure 7. Total secondary ion images from a Rhodamine B grid pattern were acquired with a CCD camera for a grid pattern with a pitch of (a) 63 µm and (b) 102 µm.

Conclusions

This paper describes the design of and presents first data from a new SIMS instrument developed for microscope-mode imaging mass spectrometry. The instrument's defocussed C_{60}^{+} PI beam can be as large as 2.5 mm^2, greatly expanding the detection area relative to previously reported SIMS microscope instrumentation [23]. We have so far attained a spatial resolution of 23.8 ± 8.2 µm using a static extraction field and a CCD camera to image the phosphor screen of our ion detector, imaging a sample area of ~1.86 mm^2. Simulations using the present configuration show that implementing a lower energy PI beam would enable an area of 20 mm^2 to be irradiated. Changing the shape of the extraction plate and adding deflectors in the ToF region would enable us to further improve the field of view we can detect.

The best mass resolution achieved experimentally is ~500 using a single field PEDA and for a mass of 687 u. However, we are fully aware of some of the factors in our experimental set up that are limiting this and making it difficult to optimise further. Simulations with the same extraction optics but without the limitations of the current detector suggest that we should be able to obtain >20,000 mass resolution in the future. By upgrading the phosphor screen of the ion detector and moving to a Timepix 3 cameras, we aim to overcome these limitations and move closer to the predicted mass resolution. In addition, improved position sensitive cameras would allow a greater repetition rate (scans per second) increasing the speed and sensitivity of detection. Further improvements to the mass resolution could be achieved by modifying the extraction optics and using a reflectron tube[28]. Despite the current limitations, the work presented here demonstrates the potential of a novel microscope mode SIMS instrument, with the capability of achieving mass spectral images of a 2.5 mm^2 area in seconds, but with comparable mass resolution and spatial resolution to microprobe SIMS. A very promising experimental setup for achieving high throughput mass spectrometry imaging.

Acknowledgements

The Rosalind Franklin Institute is grateful to funding from the UK Research and Innovation through the Engineering and Physical Sciences Research Council (EPSRC). MB and CV are grateful to the EPSRC through programme grants EP/L005913/1. EP/T021675/1 and EP/V026690/1. M. Bu. gratefully acknowledges the support of EPSRC grants EP/S028617/1 and EP/L005913/1.

References

1. Hill, R.; Blenkinsopp, P.; Thompson, S.; Vickerman, J.; Fletcher, J. S., A new time-of-flight SIMS instrument for 3D imaging and analysis. *Surface and Interface Analysis* **2011,** *43* (1-2), 506-509.
2. J.-M. Rouberol, J. G., P. Deschamps, J.-P. et Dagnot & J.-M. Guyon de la Berge Microanalyse par émission ionique secondaire. *Microscopie* **1962** *1*,395-410.
3. Castaing, R.; Slodzian, G., Microanalysis using secondary ion emission. *J Mass Spectrom* **2021,** *56* (12), e4800.
4. Luxembourg, S. L.; Mize, T. H.; McDonnell, L. A.; Heeren, R. M., High-spatial resolution mass spectrometric imaging of peptide and protein distributions on a surface. *Anal Chem* **2004,** *76* (18), 5339-44.
5. Klerk, L. A.; Altelaar, A. F. M.; Froesch, M.; McDonnell, L. A.; Heeren, R. M. A., Fast and automated large-area imaging MALDI mass spectrometry in microprobe and microscope mode. *International Journal of Mass Spectrometry* **2009,** *285* (1-2), 19-25.
6. Brouard, M.; Johnsen, A. J.; Nomerotski, A.; Slater, C. S.; Vallance, C.; Yuen, W. H., Application of fast sensors to microscope mode spatial imaging mass spectrometry. *Journal of Instrumentation* **2011,** *6* (01), C01044-C01044.
7. Nomerotski, A.; Adigun-Boaye, S.; Brouard, M.; Campbell, E.; Clark, A.; Crooks, J.; John, J. J.; Johnsen, A. J.; Slater, C.; Turchetta, R.; Vallance, C.; Wilman, E.; Yuen, W. H., Pixel imaging mass spectrometry with fast silicon detectors. *Nuclear Instruments and Methods in Physics Research Section A: Accelerators, Spectrometers, Detectors and Associated Equipment* **2011,** *633*, S243-S246.
8. Schueler, B. W., Microscope imaging by time-of-flight secondary ion mass spectrometry. *Microscopy Microanalysis Microstructures* **1992,** *3* (2-3), 119-139.
9. Schueler, B.; Sander, P.; Reed, D. A., A time-of-flight secondary ion microscope. *Vacuum* **1990,** *41* (7-9), 1661-1664.
10. Klerk, L. A.; Lockyer, N. P.; Kharchenko, A.; MacAleese, L.; Dankers, P. Y.; Vickerman, J. C.; Heeren, R. M., C60+ secondary ion microscopy using a delay line detector. *Anal Chem* **2010,** *82* (3), 801-7.
11. Froesch, M.; Luxembourg, S. L.; Verheijde, D.; Heeren, R. M., Imaging mass spectrometry using a delay-line detector. *Eur J Mass Spectrom (Chichester)* **2010,** *16* (1), 35-45.
12. Yoshimura, H.; Hazama, H.; Aoki, J.; Toyoda, M.; Naito, Y.; Awazu, K., Evaluation of a Delay-Line Detector Combined with Analog-to-Digital Converters as the Ion Detection System for Stigmatic Imaging Mass Spectrometry. *Japanese Journal of Applied Physics* **2011,** *50* (5).
13. Brouard, M.; Halford, E.; Lauer, A.; Slater, C. S.; Winter, B.; Yuen, W. H.; John, J. J.; Hill, L.; Nomerotski, A.; Clark, A.; Crooks, J.; Sedgwick, I.; Turchetta, R.; Lee, J. W.; Vallance, C.; Wilman, E., The application of the fast, multi-hit, pixel imaging mass spectrometry sensor to spatial imaging mass spectrometry. *Rev Sci Instrum* **2012,** *83* (11), 114101.
14. Nomerotski, A.; Brouard, M.; Campbell, E.; Clark, A.; Crooks, J.; Fopma, J.; John, J. J.; Johnsen, A. J.; Slater, C.; Turchetta, R.; Vallance, C.; Wilman, E.; Yuen, W. H., Pixel Imaging Mass Spectrometry with fast and intelligent Pixel detectors. *Journal of Instrumentation* **2010,** *5* (07), C07007-C07007.
15. John, J. J.; Brouard, M.; Clark, A.; Crooks, J.; Halford, E.; Hill, L.; Lee, J. W. L.; Nomerotski, A.; Pisarczyk, R.; Sedgwick, I.; Slater, C. S.; Turchetta, R.; Vallance, C.; Wilman, E.; Winter, B.; Yuen, W. H., PImMS, a fast event-triggered monolithic pixel detector with storage of multiple timestamps. *Journal of Instrumentation* **2012,** *7* (08), C08001-C08001.
16. Llopart, X.; Ballabriga, R.; Campbell, M.; Tlustos, L.; Wong, W., Timepix, a 65k programmable pixel readout chip for arrival time, energy and/or photon counting measurements. *Nuclear Instruments and Methods in Physics Research Section A: Accelerators, Spectrometers, Detectors and Associated Equipment* **2007,** *581* (1-2), 485-494.
17. Kiss, A.; Jungmann, J. H.; Smith, D. F.; Heeren, R. M., Microscope mode secondary ion mass spectrometry imaging with a Timepix detector. *Rev Sci Instrum* **2013,** *84* (1), 013704.

18. Jungmann, J. H.; MacAleese, L.; Visser, J.; Vrakking, M. J.; Heeren, R. M., High dynamic range bio-molecular ion microscopy with the Timepix detector. *Anal Chem* **2011,** *83* (20), 7888-94.
19. Jungmann, J. H.; Smith, D. F.; MacAleese, L.; Klinkert, I.; Visser, J.; Heeren, R. M., Biological tissue imaging with a position and time sensitive pixelated detector. *J Am Soc Mass Spectrom* **2012,** *23* (10), 1679-88.
20. Jungmann, J. H.; Smith, D. F.; Kiss, A.; MacAleese, L.; Buijs, R.; Heeren, R. M. A., An in-vacuum, pixelated detection system for mass spectrometric analysis and imaging of macromolecules. *International Journal of Mass Spectrometry* **2013,** *341-342*, 34-44.
21. Ellis, S. R.; Jungmann, J. H.; Smith, D. F.; Soltwisch, J.; Heeren, R. M., Enhanced detection of high-mass proteins by using an active pixel detector. *Angew Chem Int Ed Engl* **2013,** *52* (43), 11261-4.
22. Mathew, A.; Buijs, R.; Eijkel, G. B.; Giskes, F.; Dyachenko, A.; van der Horst, J.; Byelov, D.; Spaanderman, D. J.; Heck, A. J. R.; Porta Siegel, T.; Ellis, S. R.; Heeren, R. M. A., Ion Imaging of Native Protein Complexes Using Orthogonal Time-of-Flight Mass Spectrometry and a Timepix Detector. *J Am Soc Mass Spectrom* **2021,** *32* (2), 569-580.
23. Kiss, A.; Smith, D. F.; Jungmann, J. H.; Heeren, R. M., Cluster secondary ion mass spectrometry microscope mode mass spectrometry imaging. *Rapid Commun Mass Spectrom* **2013,** *27* (24), 2745-50.
24. Jungmann, J. H.; MacAleese, L.; Buijs, R.; Giskes, F.; de Snaijer, A.; Visser, J.; Visschers, J.; Vrakking, M. J.; Heeren, R. M., Fast, high resolution mass spectrometry imaging using a Medipix pixelated detector. *J Am Soc Mass Spectrom* **2010,** *21* (12), 2023-30.
25. Halford, E.; Winter, B.; Mills, M. D.; Thompson, S. P.; Parr, V.; John, J. J.; Nomerotski, A.; Vallance, C.; Turchetta, R.; Brouard, M., Modifications to a commercially available linear mass spectrometer for mass-resolved microscopy with the pixel imaging mass spectrometry (PImMS) camera. *Rapid Commun Mass Spectrom* **2014,** *28* (15), 1649-57.
26. Guo, A.; Burt, M.; Brouard, M., Mass-resolved ion microscope imaging over expanded mass ranges using double-field post-extraction differential acceleration. *International Journal of Mass Spectrometry* **2018,** *429*, 121-126.
27. Guo, A.; Burleigh, R. J.; Smith, N.; Brouard, M.; Burt, M., High-Resolution Ion Microscope Imaging over Wide Mass Ranges Using Electrodynamic Postextraction Differential Acceleration. *J Am Soc Mass Spectrom* **2020,** *31* (9), 1903-1909.
28. Burleigh, R. J.; Guo, A.; Smith, N.; Green, A.; Thompson, S.; Burt, M.; Brouard, M., Microscope imaging mass spectrometry with a reflectron. *Rev Sci Instrum* **2020,** *91* (2), 023306.
29. Yavor, M. I.; Pomozov, T. V.; Kirillov, S. N.; Khasin, Y. I.; Verenchikov, A. N., High performance gridless ion mirrors for multi-reflection time-of-flight and electrostatic trap mass analyzers. *International Journal of Mass Spectrometry* **2018,** *426*, 1-11.
30. Manura, D. *SIMION*, 8.2; Adaptas Solutions, LLC(Adaptas): 2006-2020.
31. Daniel Weibel, S. W., Nicholas Lockyer, Paul Blenkinsopp, Rowland Hill, and John C. Vickerman, AC60 Primary Ion Beam System for Time of Flight Secondary Ion Mass Spectrometry: Its Development and Secondary Ion Yield Characteristics. *Analytical Chemistry* **2004,** *75*.
32. Seah, M. P.; Green, F. M.; Gilmore, I. S., Relationships between cluster secondary ion mass intensities generated by different cluster primary ions. *J Am Soc Mass Spectrom* **2010,** *21* (3), 370-7.
33. Fearn, S., Characterisation of biological material with ToF-SIMS: a review. *Materials Science and Technology* **2014,** *31* (2), 148-161.
34. Boxer, S. G.; Kraft, M. L.; Weber, P. K., Advances in imaging secondary ion mass spectrometry for biological samples. *Annu Rev Biophys* **2009,** *38*, 53-74.
35. Agüi-Gonzalez, P.; Jähne, S.; Phan, N. T. N., SIMS imaging in neurobiology and cell biology. *Journal of Analytical Atomic Spectrometry* **2019,** *34* (7), 1355-1368.
36. Shard, A. G.; Green, F. M.; Brewer, P. J.; Seah, M. P.; Gilmore, I. S., Quantitative molecular depth profiling of organic delta-layers by C60 ion sputtering and SIMS. *J Phys Chem B* **2008,** *112* (9), 2596-605.

37. Aljoscha Körber, J. D. K., Britt S. R. Claes, Ron M. A. Heeren, Ian G. M. Anthony, Fast Mass Microscopy: Mass Spectrometry Imaging of a Gigapixel Image in 34 Minutes. *Analytical Chemsitry* **2022,** *94*, 14652−14658.
38. Lisa L. Haney, D. E. R., Delayed extraction for improved resolution of ion/surface collision products by time-of-flight mass spectrometry. *Analytica Chimica Acta* **1999,** *397*.
39. B. A. Mamyrin, V. I. K., D. V. Shmikk, and V. A. Zagulin, The mass-reflectron, a new nonmagnetic time-of-flight mass spectrometer with high resolution. **1973**.
40. Cubison, M. J.; Jimenez, J. L., Statistical precision of the intensities retrieved from constrained fitting of overlapping peaks in high-resolution mass spectra. *Atmospheric Measurement Techniques* **2015,** *8* (6), 2333-2345.
41. Aoki, J., Novel Ion Extraction Method for Imaging Mass Spectrometry. *J. Mass Spectrom. Soc. Jpn.* **2011,** *59*.
42. Engel, J.; Francis, S.; Roldan, A., The influence of support materials on the structural and electronic properties of gold nanoparticles - a DFT study. *Phys Chem Chem Phys* **2019,** *21* (35), 19011-19025.
43. Winter, B.; Halford, E.; Brouard, M., Velocity corrected ion extraction in microscope mode imaging mass spectrometry. *International Journal of Mass Spectrometry* **2013,** *356*, 14-23.
44. Brenes, D. A.; Postawa, Z.; Wucher, A.; Blenkinsopp, P.; Garrison, B. J.; Winograd, N., An experimental and theoretical view of energetic C(60) cluster bombardment onto molecular solids. *Surf Interface Anal* **2013,** *45* (1), 50-53.
45. Clark, A. T.; Crooks, J. P.; Sedgwick, I.; Turchetta, R.; Lee, J. W.; John, J. J.; Wilman, E. S.; Hill, L.; Halford, E.; Slater, C. S.; Winter, B.; Yuen, W. H.; Gardiner, S. H.; Lipciuc, M. L.; Brouard, M.; Nomerotski, A.; Vallance, C., Multimass velocity-map imaging with the Pixel Imaging Mass Spectrometry (PImMS) sensor: an ultra-fast event-triggered camera for particle imaging. *J Phys Chem A* **2012,** *116* (45), 10897-903.
46. Vallance, C.; Brouard, M.; Lauer, A.; Slater, C. S.; Halford, E.; Winter, B.; King, S. J.; Lee, J. W.; Pooley, D. E.; Sedgwick, I.; Turchetta, R.; Nomerotski, A.; John, J. J.; Hill, L., Fast sensors for time-of-flight imaging applications. *Phys Chem Chem Phys* **2014,** *16* (2), 383-95.
47. Poikela, T.; Plosila, J.; Westerlund, T.; Campbell, M.; Gaspari, M. D.; Llopart, X.; Gromov, V.; Kluit, R.; Beuzekom, M. v.; Zappon, F.; Zivkovic, V.; Brezina, C.; Desch, K.; Fu, Y.; Kruth, A., Timepix3: a 65K channel hybrid pixel readout chip with simultaneous ToA/ToT and sparse readout. *Journal of Instrumentation* **2014,** *9* (05), C05013-C05013.
48. K. Amini, S. B., M. Brouard, Three-dimensional imaging of carbonyl sulfide and ethyl iodide photodissociation using the pixel imaging mass spectrometry camera. *Rev Sci Instrum* **2015,** (86).
49. Robert G. Wilson, C. W. M., and F. A. Stevie, *Secondary Ion Mass Spectrometry : A Practical Handbook for Depth Profiling and Bulk Impurity Analysis*. Wiley: New York ; Chichester, 1989.
50. Almoric, J.; Durand, M.; Seret, A.; Nicolaÿ, A.; Houel, A.; Berbezier, I.; Bozzolo, N., Implementation of Nanoscale Secondary‐Ion Mass Spectrometry Analyses: Application to Ni‐Based Superalloys. *physica status solidi (a)* **2021,** *219* (9).
51. Keren, L.; Bosse, M.; Thompson, S.; Risom, T.; Vijayaragavan, K.; McCaffrey, E.; Marquez, D.; Angoshtari, R.; Greenwald, N. F.; Fienberg, H.; Wang, J.; Kambham, N.; Kirkwood, D.; Nolan, G.; Montine, T. J.; Galli, S. J.; West, R.; Bendall, S. C.; Angelo, M., MIBI-TOF: A multiplexed imaging platform relates cellular phenotypes and tissue structure. *Sci Adv* **2019,** *5* (10), eaax5851.